An inverse geometry problem for the localization of skin tumours by thermal analysis

P W Partridge[1,2] and L C Wrobel[1]

[1] *School of Engineering and Design, Brunel University, Uxbridge, Middlesex UB8 3PH, UK*
[2] *On leave from Dept. Eng. Civil e Ambiental, Universidade de Brasilia, 70910-900 Brasilia DF, Brazil.*

Abstract

In this paper, the Dual Reciprocity Method (DRM) is coupled to a Genetic Algorithm (GA) in an inverse procedure through which the size and location of a skin tumour may be obtained from temperature measurements at the skin surface. The GA is an evolutionary process which does not require the calculation of sensitivities, search directions or the definition of initial guesses. The DRM in this case requires no internal nodes. It is also shown that the DRM approximation function used is not an important factor for the problem considered here. Results are presented for tumours of different sizes and positions in relation to the skin surface.

Keywords: Boundary Elements, Dual Reciprocity Method, Genetic Algorithm, Tumour, Thermal Problems, Inverse Problems

1 Introduction

It is well known that the body surface temperature is controlled by blood circulation, local metabolism and heat transfer between the skin and the environment [1]. It is also known that several types of tumours, *e.g.* skin or breast, can lead to an increase in local blood flow, and thus to an increase in the local temperature [2]. On the other hand, thrombosis or vascular sclerosis decreases the blood flowing to the skin, resulting in lower skin temperatures [2].

Amongst various types of non-invasive techniques for tumour detection, such as ultra-sound or MRI, thermal methods appear to be economic and safe. Non-invasive diagnostics can be performed from skin surface temperature measurements using inverse analysis techniques based on Pennes' bioheat equation, which has a known fundamental solution previously implemented in the BEM context by Chan [3]. However, herein a numerical technique is proposed based on the Dual Reciprocity Method (DRM), which has already been used for the direct solution of the bioheat equation by Liu and co-authors [1-2, 4-7]. In the present work the tumour, the location and size of which are initially unknown, is modelled as a subregion, and in addition to the nodes used to model the boundary of the tumour, no other internal points are required.

Previous work on inverse bioheat analysis has been carried out by Ren *et al*. [8], who applied the BEM to identify heat sources in biological bodies based on the simultaneous measurement of temperature and heat flux at the skin surface, and by Majchrzak and Paruch [9], who estimated the thermophysical parameters of the tumour using a least-squares algorithm based on sensitivity coefficients.

This paper makes use of a Genetic Algorithm (GA) [10,11] in an inverse BEM formulation for determining the position and size of a tumour from skin temperature measurements. The method is of an evolutionary type, requiring no initial guess about the position of the tumour and no calculations of sensitivities or search directions. The method starts from a series of binary strings, each of which contains a possible solution to the problem (position of centre and size of tumour, considered to be rectangular in shape). The initial population of strings (the chromosomes) is improved upon iteratively using a process of crossover and mutation, which numerically imitate the natural selection procedure. It should be noted that the use of domain methods such as finite elements for the solution of the bioheat equation in this way would require the generation of a mesh for each chromosome considered in the solution. The DRM, on the other hand, does not require any remeshing, the information on the size and position of the centre of the tumour contained in each chromosome being sufficient to determine the position of the elements of the subregion in each case. A simple GA as described in the literature [12] is generally adequate.

Early applications of the DRM for general engineering problems mainly used the simple linear radial basis approximation function r, but later many other alternative functions were introduced, such as the thin plate spline and augmented thin plate spline functions [13-15]. Here, it is shown that results for the problems considered are not significantly dependent on the approximation function adopted, and for most of the results presented the cubic radial basis function r^3 is employed, with linear augmentation.

The DRM formulation for the bioheat equation is considered in the next section. This is followed by some results of direct analyses which illustrate the use of the DRM and show the relationship between tumour position and size, and temperature distribution on the skin surface. Then, the inverse geometric problem is described and the results of some inverse analyses obtained with GA are presented, for several tumour sizes and positions. The advantages and limitations of the proposed technique are also discussed.

2 Application of the Dual Reciprocity Method to the bioheat equation

The bioheat or Pennes equation can be written in the following form [1-7],

$$\rho c \frac{\partial T}{\partial t} = \nabla^2 T + \frac{\omega_b \rho_b c_b}{k}(T_a - T) + \frac{Q}{k} \tag{1}$$

where ρ, c and k denote density, specific heat and thermal conductivity of tissue; ρ_b, c_b are density and specific heat of blood, ω_b is the blood perfusion rate, T_a is the arterial blood temperature and Q is the spatial heating. Eq. (1) is subject to the usual boundary conditions for thermal problems, (i) temperature prescribed $T = \overline{T}$; (ii) heat flux prescribed, $q = \overline{q}$; (iii) Convection, $q = -h_0(T - T_0)$, where h_0 is the heat transfer coefficient and T_0 is the temperature of the surrounding fluid;. (iv) Radiation, $q = -\sigma\varepsilon(T_r^4 - T^4)$, where σ is the Stefan-Boltzman constant, ε is the radiative interchange factor between the surface and the exterior ambient temperature T_r. Eq. (1) can be written, in steady state form, as

$$\nabla^2 T = -\frac{\omega_b \rho_b c_b}{k}(T_a - T) - \frac{Q}{k} = b \tag{2}$$

Eq. (2) is a Poisson-type equation with two inhomogeneous terms, the first of which is dependent on the problem variable T, the other term being a function of space only. This equation is solved using the DRM [16] in which the fundamental solution to the Laplace equation, $u^* = 1/2\pi \log(1/r)$, is employed to treat the term on the left-hand side of (2) and the inhomogeneous terms are taken to the boundary, leading to the system of equations:

$$HT - Gq = (H\hat{U} - G\hat{Q})\alpha, \tag{3}$$

where the symbols have their usual meaning [16]. As the term b is a function of the problem unknowns, Eq. (3) is written as

$$HT - Gq = (H\hat{U} - G\hat{Q})F^{-1}b \tag{4}$$

where matrix F is calculated from the definition of the approximating functions. Calling $S = (H\hat{U} - G\hat{Q})F^{-1}$, and defining $c_1 = \omega_b \rho_b c_b / k$ and $c_2 = -(\omega_b \rho_b c_b T_a - Q)/k$, then Eq. (4) can be written

$$HT - Gq = c_1 ST + c_2 S \tag{5}$$

The previous equation may be rewritten as

$$(H - c_1 S)T - Gq = c_2 S \tag{6}$$

For a direct, well-posed problem for which the entire boundary Γ is properly defined, and one boundary condition is defined for each point on the boundary, one may apply boundary conditions to Eq. (6) in the usual way to produce

$$Ax = y + d \tag{7}$$

Eq. (7) may be solved for unknown values at boundary and internal points, if these are defined.

2.1 Approximation functions

In the original work on DRM [17], the linear radial basis function r was successfully employed. Later, much research was carried out on improving the approximating functions to apply with the method. Many alternative functions such as the cubic radial basis function, r^3, the thin plate spline, $r^2 \log(r)$, and the generalization of this, the polyharmonic splines $r^{2n} \log(r)$, were suggested [14,16]. In spite of this, much recent work involving applications of the method continues to use the linear function, for example [2], which has the advantage of simplicity. Here, tests were carried out using r, r^3 and $r^2 \log r$. Results obtained using each of these functions

are found to differ little. For the examples of inverse analysis presented in Section 5, a cubic radial basis function with linear augmentation was employed.

The particular solutions for each of these approximating functions for the Laplace equation are:
$f = r$, $\hat{u} = r^3/9$; $f = r^2 \log(r)$, $\hat{u} = r^4/16\log(r) - r^4/32$; $f = r^3$, $\hat{u} = r^5/25$.

2.2 Augmentation functions

These functions were suggested in [13] and first implemented for linear elasticity in [14]. They can produce a considerable increase in accuracy when a known function b is employed, if augmentation is chosen to be of the same order as the function concerned [15]. For two-dimensional problems, if linear augmentation is employed, the terms 1, x and y (no sum) are considered together with the approximation function. Each augmentation function has its own particular solution, *i.e.* $f = 1$, $\hat{u} = (x^2 + y^2)/4$; $f = x$, $\hat{u} = x^3/6$; $f = y$, $\hat{u} = y^3/6$. The augmentation functions considered give rise to three new rows and columns in the F matrix, numbered N+L+1 to N+L+3. These three new rows and columns contain the values of 1, x and y for each node, with the final 3×3 sub-matrix containing zero entries. In the same way, three additional columns are added to the $\hat{U}$ and $\hat{Q}$ matrices, one for each of the terms considered above. Three zeros are added to the b vector at positions N+L+1 to N+L+3. More details about the implementation of augmentation functions are given in [14].

3. Direct results for different positions and sizes of tumours

Considering Fig. 1, the external boundary, ABCD or Γ_2, is a vertical section through the skin tissue, the part AD being at the skin surface while the opposite boundary BC is considered to be an internal boundary maintained at body temperature, T = 37°C. The boundaries AB and CD are truncation boundaries, due to considering a section; at these boundaries, the condition $q = 0$ is considered. If the boundary AD is assumed to have a zero flux boundary condition, this is equivalent to thermal insulation, for instance a bandage. A more realistic condition is to consider convection or radiation at this boundary, allowing for heat exchange with the environment. Again, in Fig. 1, the internal boundary or Γ_1 is considered to divide the domain into two parts, Ω_2 the healthy tissue and Ω_1 which represents the tumour. On the boundary Γ_1 the usual compatibility and equilibrium conditions apply, *i.e.* $T_1 = T_2$ and $q_1 = -q_2$. The parameters c_1 and c_2 in Eq. (5) will be different for each subregion.

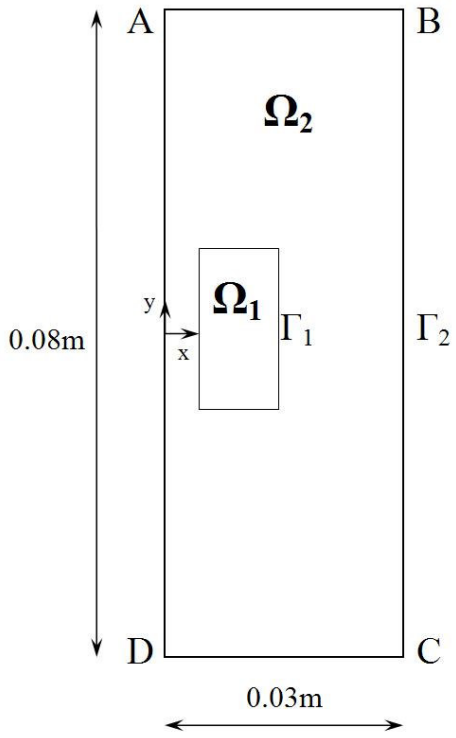

Fig. 1. Tumour within a matrix of healthy tissue

3.1 Results employing a second kind boundary condition at skin surface

With the boundary condition at the skin surface AD taken to be $q = 0$, values of the parameters necessary to calculate c_1 and c_2 are taken from [2]: ρ_b = 1000kg/m^3, c_b = 4000J/(kg ^{o}C), k = 0.5 W/(m ^{o}C). In addition, ω_b = 0.0005 ml$_b$/ml$_t$/s and Q = 420 J/(m^3 s) for healthy tissue, while the respective values for the tumour are ω_b = 0.002 ml$_b$/ml$_t$/s and Q = 4200 J/(m^3 s) [2], with the subscripts b and t indicating blood and tissue, respectively. The arterial blood temperature T_a is 37^{o}C.

Considering the geometry given in Fig. 1, in which the skin depth is considered to be 0.03m and the length of the cross-section considered is 0.08m, a discretisation is adopted with 56 linear boundary elements for Γ_2 and 16 linear elements for Γ_1. Taking both Ω_1 and Ω_2 to be healthy tissue, and assuming the boundary condition along AD to be $q = 0$, then one obtains a constant temperature of 37.14^{o}C at the skin surface. This result was checked using the BEM with internal cells instead of DRM and also using finite elements (384 triangular elements). For both this example and those that follow, no internal nodes were necessary with the DRM other than those defining Γ_1. Next, considering the subregion Ω_1 to be a tumour of thickness 0.01m and length 0.02m centred at the coordinate (0.01, 0) and employing the values of the parameters for this case given above, the temperature distribution given in Table 1 is obtained at the skin surface (boundary AD).

In order to check the influence of the approximation functions employed and the use of the augmentation functions, results are calculated for $f = r$, $f = r^3$ and $f = r^2 \log(r)$. In all three cases, results are presented for the function on its own and for the function augmented with the linear terms 1, x and y.

Table 1: Temperature variation at the skin surface considering three approximating functions, with and without augmentation

y	$f = r$		$f = r^3$		$f = r^2 \log(r)$		FEM
	Function	with aug	Function	with aug	Function	with aug	
0.035	37.17	37.17	37.17	37.17	37.17	37.17	37.17
0.03	37.18	37.18	37.17	37.18	37.17	37.18	37.17
0.025	37.19	37.19	37.19	37.19	37.19	37.19	37.18
0.02	37.21	37.21	37.20	37.20	37.20	37.21	37.21
0.015	37.23	37.24	37.23	37.23	37.23	37.23	37.23
0.01	37.27	37.27	37.26	37.27	37.26	37.27	37.27
0.005	37.29	37.30	37.29	37.29	37.29	37.29	37.29
0.0	37.30	37.31	37.30	37.30	37.30	37.30	37.30
-0.005	37.29	37.30	37.29	37.29	37.29	37.29	37.29
-0.01	37.27	37.27	37.26	37.27	37.26	37.27	37.27
-0.015	37.23	37.24	37.23	37.23	37.23	37.23	37.23
-0.02	37.21	37.21	37.20	37.20	37.20	37.21	37.21
-0.025	37.19	37.19	37.19	37.19	37.19	37.19	37.18
-0.03	37.18	37.18	37.17	37.18	37.17	37.18	37.17
-0.035	37.17	37.17	37.17	37.17	37.17	37.17	37.16

Finite element results obtained using a 384 triangular element mesh are also included. It can be seen that results differ very little between the different approximation functions. It can also be seen that the results for any function including augmentation are very similar and agree very well with the finite element results. Given the above, all subsequent results, including those for the inverse analysis, were obtained using $f = r^3$ with linear augmentation.

Considering now a tumour of the same size and shape as that shown in Fig. 1 but located with its centre at position (0.02, 0.02), the results for temperature distribution at the skin surface are given in Fig. 2. Note that the temperature variation is no longer symmetric since the tumour is no longer centred on $y = 0$.

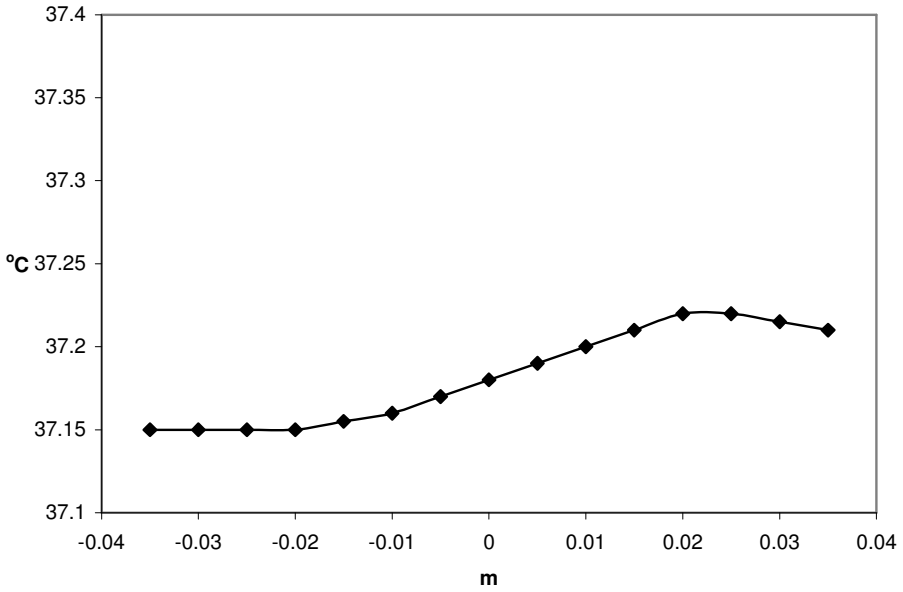

Fig. 2. Skin surface temperature distribution for tumour of size 0.01 × 0.02m centred at position (0.02, 0.02)

In addition to considering different positions of the tumour, different sizes may also be considered. In Fig. 3, the tumour denoted A is of size 0.005m × 0.01m, *i.e*. one half the size considered in the previous case. The centre is at position (0.005, 0.020). The tumour denoted B is of the same size as A, but centred at position (0.02, 0.02). The tumour denoted C is of size 0.0175m × 0.035m (1¾ the size of the original tumour) and is centred at position (0.01625, 0). Results for the surface temperature variation for all of these cases are given in Fig. 4.

Note that tumours A and B are of the same size, but as A is near the surface, a significant peak appears in the curve. Curve B is nearly flat, while tumour C, whilst far from the surface, has a bigger size, thus also giving rise to a significant peak in the temperature distribution.

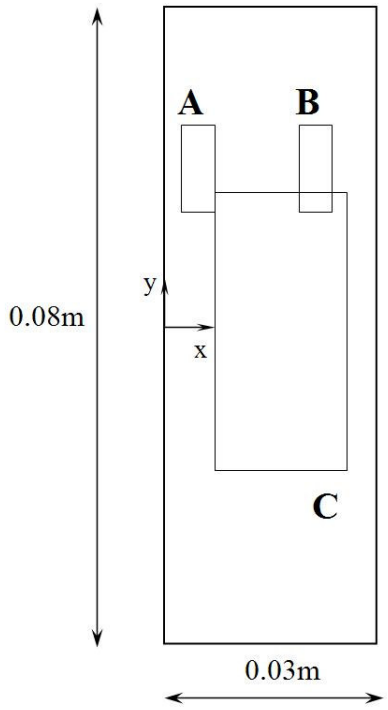

Fig. 3. Tumours of different sizes and positions

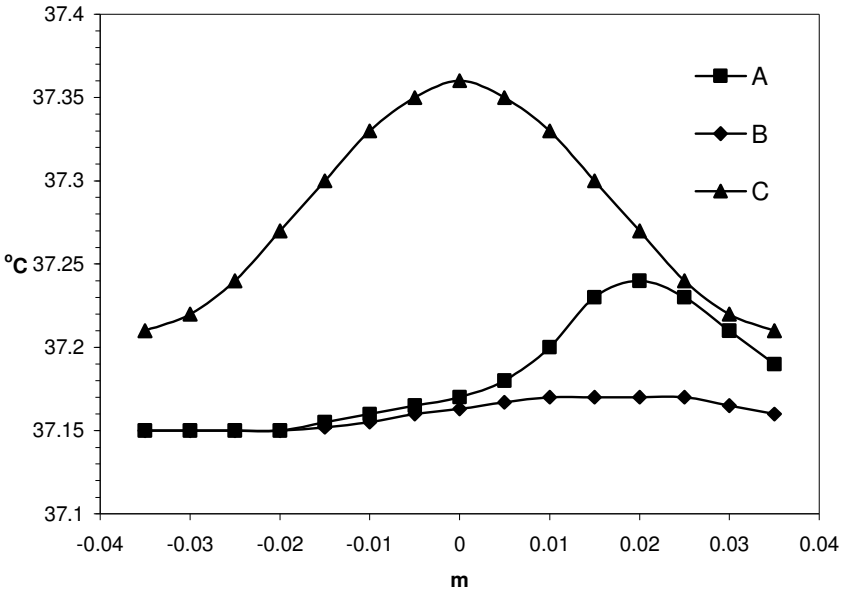

Fig. 4. Variation of skin surface temperatures for the tumours shown in Fig. 3 A-C

3.2 Results employing a third kind boundary condition at the skin surface

It has been previously mentioned that instead of considering a second kind boundary condition at the skin surface, it would be more realistic to consider convection and radiation. In [2], a linearised radiation condition is employed, considering that the temperatures in question are small and the combined convection/radiation condition written as:

$$q = -h_0 (T - T_0) - h_r (T - T_{env}) \tag{8}$$

Considering $T_{env} = T_0$, one can write (8) as $q = -h_{eff} (T - T_0)$. The relevant parameters are taken as $h_{eff} = h_0 + h_r = 10 \text{W/m}^2$ and $T_0 = 25^{\text{o}}\text{C}$ [2]. With the above data, the combined condition was considered at the skin surface for healthy tissue (c_1 and c_2 values constant for the whole of the region shown in Fig. 1). The results show an average temperature of 36.36^{o}C at the skin surface, with some minor perturbations near the two ends due to the treatment of the corners in the DRM formulation. This lower temperature value is consistent with the exchange of heat to a colder environment. Table 2 shows results using the combined convection/radiation condition for the tumour of size 0.01x 0.02m centred at (0.01, 0). The temperature values obtained are also lower than those obtained before, however a peak is still observed which enables the temperature distribution to be used for the detection of tumours.

Table 2: Temperatures at skin surface for the configuration shown in Fig. 1, for convective boundary condition at skin surface

y	*T*
0.035	36.40
0.03	36.41
0.025	36.42
0.05	36.48
0.015	36.59
0.01	36.72
0.005	36.83
0.	36.87
-0.005	36.83
-0.01	36.72
-0.015	36.59
-0.02	36.48
-0.025	36.42
-0.03	36.41
-0.035	36.40

Results in Fig. 5 are given for the skin temperature distribution for a tumour of size 0.01 × 0.02m, centred at (0.02, 0.02) (case D), and also one of 0.005 × 0.001m, centred at (0.005, 0.02) (case E), for the convective boundary condition considered above.

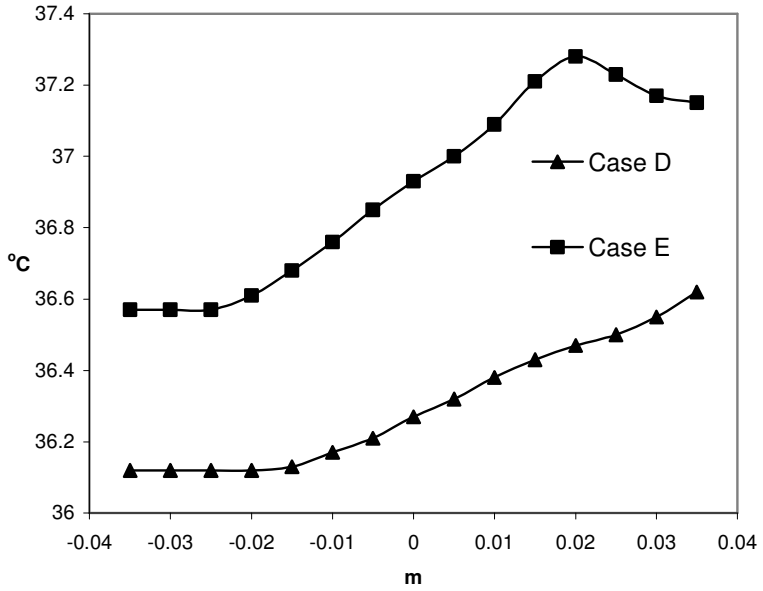

Fig. 5. Temperatures at skin surface for cases D and E for convective boundary condition at skin surface

4. Procedure for the determination of the size and position of tumours from skin surface temperatures using Genetic Algorithm

Genetic algorithms [10,11] are ideally suited to the optimization problem of obtaining the position of a tumour. The method is of an evolutionary type, based on the process of natural selection, requiring no initial guess about tumour position, and no calculation of derivatives, sensitivities or directions in which to search. Here, a simple GA as detailed in [12] is employed. The geometry of each tumour is considered to be rectangular, as in [2]. The number and size of the initial population of chromosomes is defined by using Fig. 6, in which the space to be searched is defined. The cross-section is 0.03m thick and 0.08m long. The basic tumour size is that given in Fig. 1, *i.e.* 0.01 × 0.02m; this basic size will be referred hereafter as size 1. Larger tumours will be of sizes greater than 1, while smaller tumours will be of size less than 1. For example, a tumour of size 0.02 × 0.04m (double the size of the tumour considered in Fig. 1) is considered to be of size 2, while a tumour of size 0.005 × 0.01m (half the size of the tumour considered in Fig. 1) is considered to be of size 0.5.

The information stored in each chromosome corresponds to the coordinates x and y of the centre of the tumour and its size, as defined above. As three pieces of information are involved, each chromosome has three alleles. It is necessary to define the number of binary digits to define each allele, the total size of each chromosome being the sum of the sizes of each allele. Considering a tumour of size 1 and referring to Fig. 6, the search area for the position of the centre of the tumour is restricted to the shaded area as the centre can only come within a certain distance of the boundaries,

since the tumour must stay within the defined space. The search space is thus 0.02 × 0.06m.

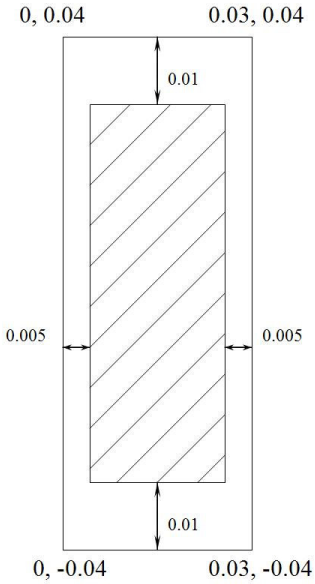

Fig. 6. Search area for the position of the centre of tumour of size 1

Considering the boundary element model discussed in the last section, 12 elements were defined over the thickness, giving a distance of 0.0025m between nodes. In order to obtain a significantly smaller distance between two adjacent binary values of the allele, 5 binary digits will be considered, having values from 00000 to 11111. The value 00000 corresponds to the left margin in Fig. 6, and the value 11111 to the right one. Dividing 0.02 by 31 (equal to 2^5 -1) gives 0.00064516, which is thus the distance between two adjacent binary values of this allele. As an example, for the binary value 01011, the x coordinate of the centre is 11×0.00064516 = 0.00709676. A value of 0.005 due to the edges in Fig. 6 must be added to the result, and the x coordinate of the centre indicated by this value of the allele is then 0.01209676. Using a similar reasoning in the y direction, 7 binary digits are employed for the allele, the distance between two adjacent values is 0.06 divided by 127 (2^7 -1) = 0.00047244, and the value 0.04 must be added to take into account the edge position.

The final allele defines the size of the tumour. Considering 3 binary digits, from 000 to 111, it is considered that 000 corresponds to ¼ of the size of the tumour shown in Fig. 1. Each binary value then doubles that size in steps of ¼, to a maximum of twice the size of the original tumour in Fig. 1 for the binary value 111. The basic tumour of size 1 thus corresponds to the binary number 011. Considering the above, one can write

$$\begin{aligned} x_c &= a_x \times A_1 + b_x \\ y_c &= a_y \times A_2 + b_y \end{aligned} \tag{9}$$

where A_1, A_2 are the values of the first two alleles in base 10. The values a_x, b_x and a_y, b_y were given above for the case of a size 1 tumour, and values for other sizes are given in Table 3. Summing the sizes of the three alleles, the total size of the chromosome is 15 binary digits.

Table 3: Parameters for relating values of alleles with the position of the centre of the tumour

Size	a_x	b_x	a_y	b_y
0.25	0.00088709	0.00125	0.00059055	0.0375
0.50	0.00080645	0.0025	0.00055118	0.035
0.75	0.00072580	0.00375	0.00051181	0.0325
1.00	0.00064516	0.005	0.00047244	0.03
1.25	0.00056451	0.00625	0.00043307	0.0275
1.50	0.00048387	0.0075	0.00039370	0.025
1.75	0.00040322	0.00875	0.00035433	0.0225
2.00	0.00032258	0.01	0.00031496	0.02

The population size was fixed at 20, which is within the guidelines established by Kahn [18] who suggested that this value should be between ℓ and 2ℓ, where ℓ is the size of the chromosome. After establishing an initial population, the position and size of the tumour for each chromosome is obtained as considered above, and results for the temperature distribution at nodes along the part AD of the Γ_2 boundary (Fig. 1) are calculated using the DRM algorithm. For the DRM discretisation, the elements on the boundary Γ_2 (Fig. 1) are fixed and those on Γ_1 are given for a size 1 tumour centred at position (0.01, 0). Therefore, it is only necessary to multiply by the size and sum to the coordinates the values given by Eq. (9).

The objective of the algorithm is to minimise the value of the sum of the squares of the differences between the temperatures calculated at nodes on side AD (Fig. 1) and the measured values. The chromosomes are ordered according to the value of the sum of the squares, with the smallest value first, the position in this new order being referred to as the fitness. Individuals are selected for crossover using the roulette wheel method described by Goldberg [10], the fitter individuals having the greater probability of selection. Two point crossover and mutation with a probability of 1% is carried out in the GA. A process of elitism is employed by which the best individual from one generation passes automatically to the next, in order to ensure that the best solution is not lost [10]. A maximum of 100 generations is permitted; if the process has not converged after this, iterations are halted. The stopping criterion considered is that 80% of individuals must converge to the same value.

5. Some results for the identification of the position and size of tumours

Considering the same geometry as in the previous examples of direct analyses, shown in Figs 1 and 6, in which a section of tissue of dimensions 0.03m × 0.08m was considered, and using their results as input data for the inverse analysis, the

temperature values for part AD of Γ_2 can be calculated. These values are compared with the values calculated for each size and position of tumour indicated by the chromosomes in the GA, and the sum of the squares of the differences minimised. The boundaries Γ_1 and Γ_2 are discretised with 16 and 56 linear boundary elements, respectively.

5.1 Results considering the skin surface to have a second kind boundary condition

Case 1 In this case, the data for the measured temperatures at the skin surface were those given in Table 1 for the function $f = r^3$ with augmentation. The results produced by the inverse analysis were tumour centre at position (0.00952, -0.00024) and size 1. Results converged in 30 generations. The data used to generate the results given in Table 1 were centre (0.01, 0) and size 1.

Case 2 In this case, the data for the measured temperatures on the skin surface were as given in Fig. 2. Results produced by the program were tumour centre at position (0.02048, 0.01915) and size=1. Results converged in 57 generations. The data used to generate the results given in Fig. 2 were centre (0.02, 0.02) and size 1.

Cases 3-5 Considering as input data for the temperature distribution at the skin surface the values given in Fig. 4A, the results produced by the program were tumour centre at position (0.00653, 0.01957) and size 0.5. Results converged in 75 generations. The data used to generate the results given in Fig. 4A were centre (0.005, 0.02) and size 0.5. Considering Fig. 4C, the results obtained by the inverse analysis were tumour centre at position (0.01681, -0.00088) and size 1.75. The data used to generate curve 4C were centre (0.016, 0) and size 1.75.

The inverse analysis did not converge for the data in Fig. 4B. The skin surface temperature variation produced by this tumour (curve 4B) was nearly flat. The physical interpretation of this temperature variation is that the tumour is too small and too far from the skin surface to produce any significant skin temperature variation, therefore it cannot be detected by using the current GA algorithm.

5.2 Results considering the skin surface to have a third kind boundary condition

Case 6 Considering as input data on the skin surface the results given for the tumour in Table 2, the results produced by the inverse analysis were tumour centre at position (0.01016, 0.00118) and size 1. Results converged in 27 generations. The data used to generate the results given in Table 2 were centre (0.01, 0) and size 1.

Cases 7-8 Considering as input data on the skin surface the results given in Fig. 5D, the results produced by the inverse analysis were tumour centre at position (0.02093, 0.01927) and size 1. The data used to generate curve 5D were centre (0.02, 0.02) and size 1. Results converged in 24 generations. Considering as input data on the skin surface the results given in Fig. 5E, the results produced by the inverse analysis were tumour centre at position (0.00564, 0.01960) and size 0.5. The data used to generate curve 5E were centre (0.005, 0.02) and size 0.5.

5.3 Evolution of GA results

This section discusses the evolution and convergence of the GA results for two of the above cases. Considering first Case 1, as the initial population in the GA is generated randomly, the predicted values of tumour centre (positions x_c and y_c) display a large scatter, as shown in Fig. 7a. There is a substantial improvement after ten generations (Fig. 7b), and the process is considered to have converged after thirty generations (Fig. 7c), with 80% of the solutions producing the same values x_c = 0.00952, y_c = -0.00024, compared to the correct solution x_c = 0.01, y_c = 0. By continuing the evolution process, 100% convergence to the position x_c = 0.00952, y_c = -0.00024 was achieved after 43 generations (Fig. 7d).

A similar pattern is displayed for Case 7 in Fig. 8, with a large scatter of results for the initial population (Fig. 8a), considerable improvement after ten generations (Fig. 8b), and convergence after thirty four generations (Fig. 8c), with 80% of the solutions producing the same values x_c = 0.0209, y_c = 0.0192, compared to the correct solution x_c = 0.02, y_c = 0.02.

5.4 Results for Noisy Data

Case 1 above was reanalysed by introducing some noise in the skin surface temperature measurements. The error for electrical thermometers used for measuring human body temperature has been quoted as $\pm 0.05^{o}$C or less [19]. The skin surface temperature data was initially perturbed by the addition of Gaussian random variables of zero mean and standard deviation σ = 0.01 to the data displayed in the fifth column of Table 1. Although these errors do not seem significant, the temperature differences in Table 1 are so small that the effect of this added noise substantially perturbs the corresponding curve. In spite of this, a tumour could still be identified after 30 generations, centred at the position x_c = 0.0191, y_c = 0.0002, compared to the correct solution x_c = 0.01, y_c = 0. Consistent with the flatter skin temperature distribution, the tumour was identified as having size 1½, bigger than the original tumour of size 1.

The problem was also analysed with noisy data of standard deviation σ = 0.05, in which case the perturbations added to the skin temperature variation curve are even more significant. The identified position of the tumour in this case was x_c = 0.0212, y_c = -0.0005, with size 1¾. Convergence of the GA was obtained after 33 generations.

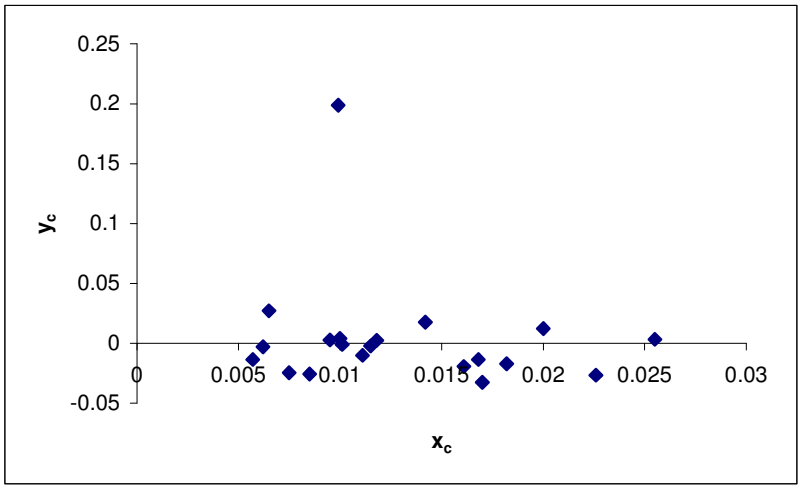

a. Initial population

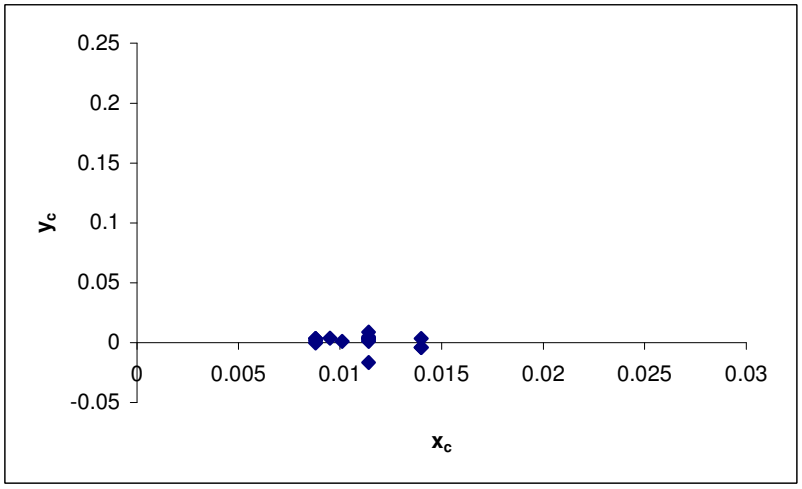

b. Generation 10

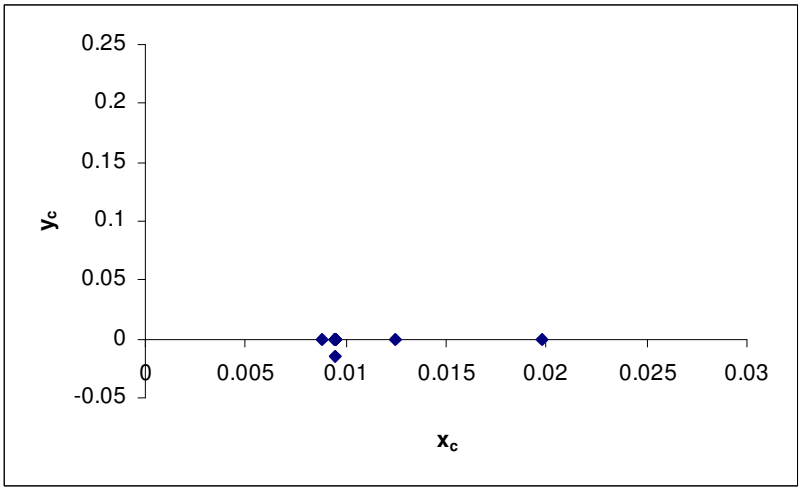

c. Generation 30

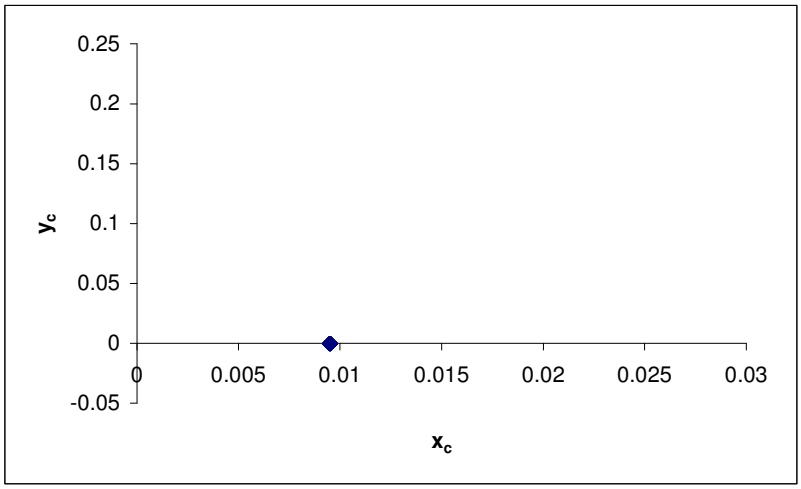

d. Generation 43

Fig. 7. Convergence of the GA results for Case 1

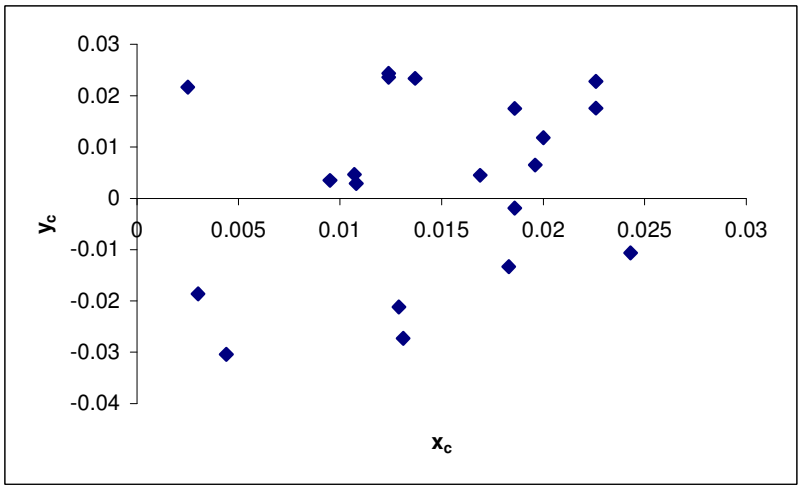

a. Initial population

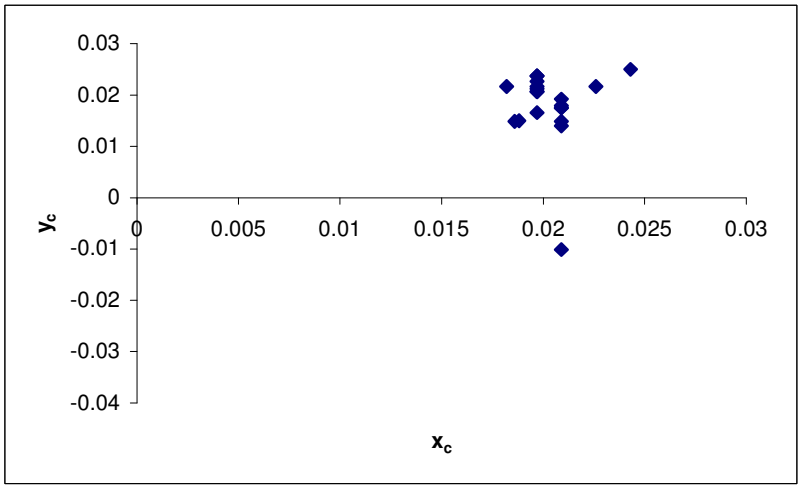

b. Generation 10

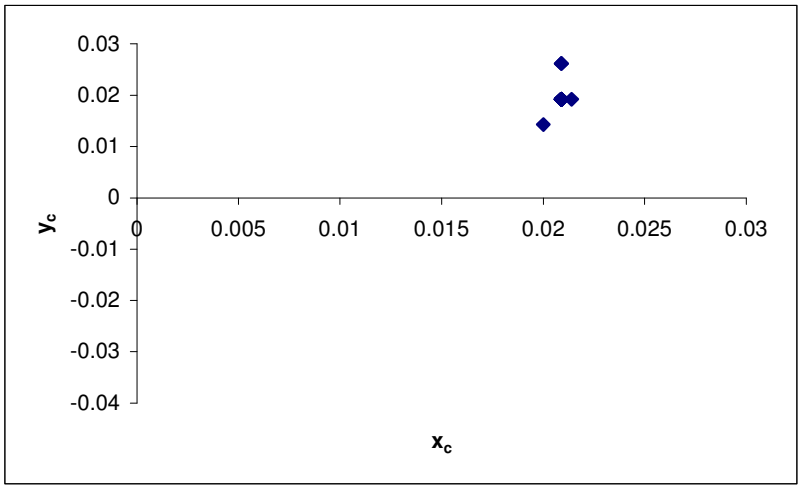

c. Generation 24

Fig. 8. Convergence of the GA results for Case 7

6. Conclusions

In the above, a numerical technique based on the dual reciprocity boundary element method coupled with a genetic algorithm was used in an inverse procedure for obtaining the position and size of tumours from temperature data on the skin surface. The procedure has the advantage of not needing to calculate derivatives or sensitivities, and does not require an initial estimate of the position of the tumour. It is seen, however, that tumours that are very small or deeply located produce only a small perturbation of the skin temperature variation, and thus cannot be detected in this way. In the case of the DRM, it is seen that the approximating function adopted is not an important factor, and also that internal nodes are not necessary.

The proposed technique can be directly extended to more realistic three-dimensional inverse analysis estimations, at an increased computational cost. It can also be extended to deal with temperature-dependent blood perfusion coefficients, which are particularly relevant when considering hyperthermia cancer therapy [20,21].

Acknowledgement

The first author gratefully acknowledges the support of the Brazilian agency CAPES in funding this work.

References

[1] Deng, Z-S, Liu J, Mathematical modelling of temperature mapping over skin surface and its implementation in thermal disease diagnostics, *Computers in Biology and Medicine*, **34**:495-521, 2004.

[2] Liu J, Xu LS, Boundary information based diagnostics on the thermal states of biological bodies, *International Journal of Heat and Mass Transfer*, **43**:2827-2839, 2000.

[3] Chan CL, Boundary element method analysis of the bioheat transfer equation, *Transactions of the ASME, Journal of Biomechanical Engineering*, **114**:358-365, 1992.

[4] Deng Z-S, Liu J, Parametric studies on the phase shift method to measure the blood perfusion of biological bodies, *Medical Engineering & Physics*, **22**:693-702, 2000.
[5] Liu J, Xu LX, Estimation of blood perfusion using phase shift in temperature response to sinusoidal heating at skin surface, *IEEE Transactions on Biomedical Engineering*, **46**:1037-1043, 1999.
[6] Lu W-Q, Liu J, Zeng Y, Simulation of the thermal wave propagation in biological tissues by the dual reciprocity boundary element method, *Engineering Analysis with Boundary Elements*, **22**:167-174, 1998.
[7] Deng Z-S, Liu J, Modelling of multidimensional freezing problem during cryosurgery by the dual reciprocity boundary element method, *Engineering Analysis with Boundary Elements*, **28**:97-108, 2004.
[8] Ren ZP, Liu J, Wang CC, Boundary element method for solving normal or inverse bio-heat transfer problem of biological bodies with complex shape, *Journal of Thermal Science*, **4**:117-124, 1995.
[9] Majchrzak E, Paruch M, Identification of the tumour region on the basis of skin surface temperature, Proceedings ECCOMAS 2004, Eds P. Neittaanmaki, T. Rossi, K. Majava and O. Pironneau, 1-14, 2004.
[10] Goldberg DE, *Genetic Algorithms in Search, Optimization and Machine Learning*, Addison Wesley, 1989.
[11] Goldberg DE, Zakrewsky K, Sutton B, Gadient R, Chong C, Galego P, Miller B, Cantu-Paz E, Genetic algorithms: A bibliography, Technical Report 97011, 1999.
[12] Castro LCLB, Partridge PW, Minimum weight design of framed structures using a genetic algorithm considering dynamic analysis, *Latin American Journal of Solids and Structures*, **3**:107-123, 2006.
[13] Golberg MA, Chen CS, The theory of radial basis functions applied to the BEM for inhomogeneous partial differential equations, *Boundary Element Communications*, **5**:57-61, 1994.
[14] Bridges TR, Wrobel LC A DRM formulation for elasticity problems with body forces using augmented thin plate splines, *Communications in Numerical Methods in Engineering*, **12**:209-220, 1996.
[15] Partridge PW, Towards criteria for selecting approximation functions in the dual reciprocity method, *Engineering Analysis with Boundary Elements*, **24**:519-529, 2000.
[16] Partridge PW, Wrobel LC, Brebbia CA, *The Dual Reciprocity Boundary Element Method*, Elsevier, 1992.
[17] Nardini D, Brebbia CA, A new approach to free vibration analysis using boundary elements, *Applied Mathematical Modelling*, **7**:157-162, 1983.
[18] Kahn N, Population sizing in genetic and evolutionary algorithms, Internal Report, University of Illinois at Urbana Champaign, 2002.
[19] Fogelson, IB, Berdnikov, SI and Zavitkov, YV, Electrical thermometers and sensors for measuring human body temperature, *Biomedical Engineering*, **30**:211-213, 1996.
[20] Tompkins DT, Vanderby R, Klein SA, Beckman WA, Steeves RA, Frye DM, Paliwal, BR, Temperature-dependent versus constant-rate blood perfusion modelling in ferromagnetic thermoseed hyperthermia: Results with a model of the human prostate, *International Journal of Hyperthermia,* **10**:517-536, 1994.
[21] Lang J, Erdmann B, Seebass M, Impact of nonlinear heat transfer on temperature control in regional hyperthermia, *IEEE Transactions on Biomedical Engineering*, **46**:1129-1138, 1999.